Journal of the American Ceramic Society

RESEARCH ARTICLE OPEN ACCESS

Transparent Er:$(Y,La)_2O_3$ Ceramics With High La^{3+} Concentration for Mid-Infrared Laser Applications

Zehao Xu[1,2] | Hiroaki Furuse[1] | Shogo Miyoshi[1] | Tohru S. Suzuki[1,2]

[1]National Institute for Materials Science (NIMS), Tsukuba, Ibaraki, Japan | [2]Graduate School of Advanced Science and Engineering, Waseda University, Shinjuku, Tokyo, Japan

Correspondence: Hiroaki Furuse (Furuse.Hiroaki@nims.go.jp)

Received: 30 April 2026 | **Revised:** 3 July 2026 | **Accepted:** 8 July 2026

Keywords: co-precipitation | laser materials | mid-infrared | spark plasma sintering | transparent ceramics

ABSTRACT

Exploration of mid-infrared laser materials with broad emission spectra is crucial for the generation of ultrashort pulses, particularly in spectroscopic and material processing applications. The incorporation of La^{3+} ions into Er:Y_2O_3, a representative mid-infrared laser material, induces crystal lattice distortion and broadens its emission spectrum. However, the La^{3+} doping concentration is typically limited to approximately 10 at.% owing to the formation of secondary phases. In this study, transparent $(Er_{0.05}Y_{0.95-x}La_x)_2O_3$ mixed sesquioxide ceramics with high La^{3+} concentration of $x = 0.2$ was fabricated together with $x = 0$, 0.05, and 0.1 via co-precipitation and low-temperature spark plasma sintering (SPS) to investigate the effects of La^{3+} concentration on mid-infrared emission properties. Both the emission spectral width and luminescence lifetime at approximately 2700 nm increased with increasing La^{3+} concentration. For $x = 0.2$, the values were approximately 17 nm and 3.8 ms, respectively, compared to approximately 4 nm and 3.3 ms for $x = 0$. Although the $x = 0.2$ sample achieved an in-line transmittance above 80% at 2720 nm, it was still lower than those of samples with lower La^{3+} content. Microstructural analysis revealed that La^{3+} addition reduced the average grain size and formed residual pores, likely responsible for increased optical scattering. To eliminate the residual pores, post-hot isostatic pressing (HIP) treatment was conducted at various temperatures, which resulted in improved optical transmittance. We believe that optimizing processing conditions could further enhance optical quality at high La^{3+} concentrations, making it a promising candidate for mid-infrared laser applications.

1 | Introduction

The 2.7 μm laser emission of Er^{3+} ions ($^4I_{11/2} \rightarrow {}^4I_{13/2}$ transition) coincides with strong water and water vapor absorption, making Er^{3+}-doped laser gain media promising candidates for medical surgery, spectroscopic, and materials processing [1–3]. Among various host materials, cubic sesquioxide groups, such as Y_2O_3, Lu_2O_3, and Sc_2O_3, are particularly promising for mid-infrared laser emission owing to their high thermal conductivity, low phonon energy, large Stark splitting, and excellent thermo-mechanical properties [4, 5]. For ultrashort pulse lasers, broadband gain media are highly desirable, as smooth and broad emission bands are essential for achieving shorter pulse durations [6]. Mixed sesquioxides, such as $(Lu,Sc)_2O_3$ and $(Y,Sc)_2O_3$, have shown enhanced emission bandwidths and compositional spectral tuning due to intrinsic crystal field disorder arising from the mismatch in cation radii among trivalent ions (Y^{3+}: 0.90 Å, Lu^{3+}: 0.86 Å, Sc^{3+}: 0.75 Å) [7, 8].

While Er^{3+}-doped mixed sesquioxides exhibit broader emission bands than single sesquioxide hosts, further spectral broadening is desirable for ultrashort-pulse mid-infrared lasers [7–12]. In the $(Y,La)_2O_3$ system, the substantial cation radius difference between Y^{3+} (0.90 Å) and La^{3+} (1.03 Å) [13, 14] is expected to

induce stronger local lattice distortion and modifications of the crystal-field environment, subsequently impacting the emission properties of Er^{3+} ions. Moreover, the relatively lower phonon energy of La_2O_3 (~400 cm^{-1}) [15, 16] compared to Y_2O_3 (591 cm^{-1}), Lu_2O_3 (612 cm^{-1}), and Sc_2O_3 (672 cm^{-1}) [17] suggests that $(Y,La)_2O_3$ mixtures may achieve the relatively lower phonon energy, potentially reducing non-radiative relaxation and then enhancing laser efficiency. Nonetheless, the melting point of sesquioxides, which typically exceeds 2400°C, poses a significant challenge for single crystal synthesis and consequently impedes large-scale commercial production [18, 19]. By contrast, ceramic processing can produce transparent bulk ceramics below their melting points with more homogeneous doping of laser-active ions [4, 20].

Sun et al. demonstrated high transparency and strong laser emission at 2715 and 2727 nm from $Er:(Y_{0.9}La_{0.1})_2O_3$ ceramics fabricated by hot pressing at 1700°C [21]. Balabanov et al. also fabricated $(Er_{0.07}Y_{0.83}La0_{.1})_2O_3$ ceramics with a transmittance of 80% by vacuum sintering and observed additional spectral broadening in the mid-infrared absorption and emission bands compared to $Er:Y_2O_3$ ceramics [22].

La^{3+} doping effectively enhanced the emission capability of Er^{3+} ions in $Er:Y_2O_3$ system. However, to the best of our knowledge, La^{3+} concentrations exceeding 10 at.% have rarely been reported in previous studies. This limitation likely arises from the formation of secondary phases such as monoclinic or perovskite phases, when solubility or temperature limits are exceeded in the Y_2O_3-La_2O_3 solid solution system [23–27]. Such phase formation is considered the primary obstacle to fabricating transparent ceramics. Therefore, investigating fabrication processes to achieve optical transparency in $Er:(Y,La)_2O_3$ ceramics with high La^{3+} content and examining the effect of elevated La^{3+} concentrations on luminescence properties are of considerable interest.

Spark plasma sintering (SPS) is an advanced sintering technique that enables fabrication of dense ceramics with fine microstructures at relatively lower sintering temperatures than conventional pressure-less vacuum sintering [28–32]. By employing SPS, transparent rare earth doped Y_2O_3 ceramics with grain sizes around several 100 nm have been developed [33–36], and these materials have been applied to laser materials and a saturable absorber in the mid-infrared region [36]. This approach is also considered effective for avoiding secondary phase formation in $(Y,La)_2O_3$ ceramics that would otherwise occur during high-temperature heat treatment. Additionally, co-precipitation has been reported as an effective method for preparing fine powders with high doping concentrations and has the potential to overcome solid solubility limitations caused by diffusion constraints in traditional solid-state reaction methods [37, 38]. Thus, combining SPS with co-precipitated powders provides an efficient strategy to suppress secondary phase formation in $(Y,La)_2O_3$ ceramics and achieve transparent ceramics for laser applications.

In this study, we investigated the fabrication of transparent Er^{3+} doped $(Y,La)_2O_3$ mixed sesquioxide ceramics with high La^{3+} content via co-precipitation followed by SPS and hot isostatic pressing (HIP) treatments. We systematically investigated the effects of high La^{3+} content on the microstructure, optical properties, and emission behavior of these potential mid-infrared laser materials.

2 | Experimental Procedure

2.1 | Material Preparation

Figure 1 shows a schematic of the experimental procedure. High-purity yttrium nitrate hexahydrate, lanthanum nitrate hexahydrate, and erbium chloride hexahydrate were used as starting materials and dissolved in deionized water according to the stoichiometric ratio of $(Er_{0.05}Y_{0.95-x}La_x)_2O_3$ (x = 0, 0.05, 0.1, 0.2). Analytical-grade ammonium bicarbonate was used as the precipitant and diluted with deionized water. The precipitant solution was dripped into the mixed metal ion solution under stirring. After precipitation, the solution was continuously stirred and aged for approximately 12 h. The precursor was collected by centrifugation, washed several times with deionized water, and dried. Finally, the precursor was calcined at 1200°C for 2 h in air.

After sieving, the powder was subjected to SPS (LABOX-325, Sinter Land, Japan) under vacuum. The temperature was monitored using a pyrometer. The sintering temperature, heating rate, and holding time were 1300°C, 5°C/min, and 1 h, respectively. An applied pressure of 80 MPa was preloaded and maintained constantly until completion of the sintering process. After SPS, the sintered ceramics were annealed in air, and both surfaces were polished for characterization. Three sets of HIP treatments for SPSed samples were conducted using a HIP furnace (O_2-Dr. HIP, Kobe Steel, Japan) under Ar pressure of 180 MPa at 1200°C, 1300°C, and 1400°C for 2 h, respectively.

2.2 | Characterization

For material characterization, the phase compositions of the powders and sintered ceramics were measured using an X-ray diffractometer (Ultima IV, Rigaku Co., Japan). To evaluate the phonon energies of the host materials, Raman shift spectra were recorded using a Raman microscope (inVia Reflex, Renishaw Co., UK) with a 785 nm laser for undoped Y_2O_3 and $(Y_{0.8}La_{0.2})_2O_3$ calcinated powders to avoid absorption owing to Er^{3+} ions. The in-line optical transmittance of the ceramics was measured using a UV-VIS-NIR spectrometer (UV-3600i Plus, Shimadzu Co., Japan). The morphologies of the powders and the microstructures of the sintered ceramics were observed using a field-emission scanning electron microscope (S-4800, Hitachi Co., Japan). To examine the microstructure of the sintered ceramics, the polished surfaces were thermally etched at 900°C for 1 h.

2.3 | Luminescence Properties

The luminescence spectra and decay curves were obtained using a 976 nm laser diode as the excitation source. Mid-infrared luminescence spectra and temporal decay curves were measured using an optical spectrum analyzer (OSA205C, Thorlabs Co., USA) and an InAsSb detector, respectively.

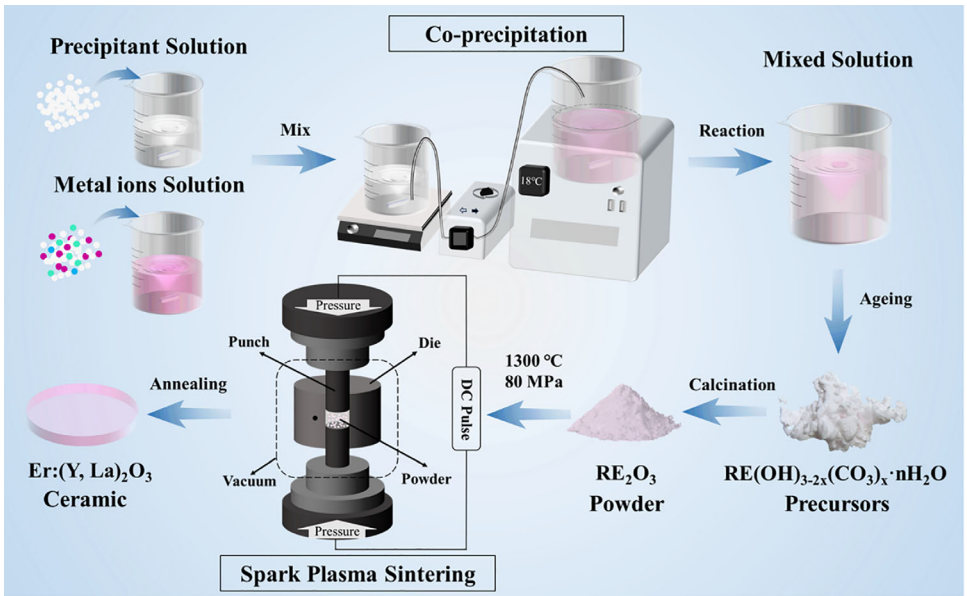

FIGURE 1 | Experimental procedure for fabricating $(Er_{0.05}Y_{0.95-x}La_x)_2O_3$ transparent ceramics.

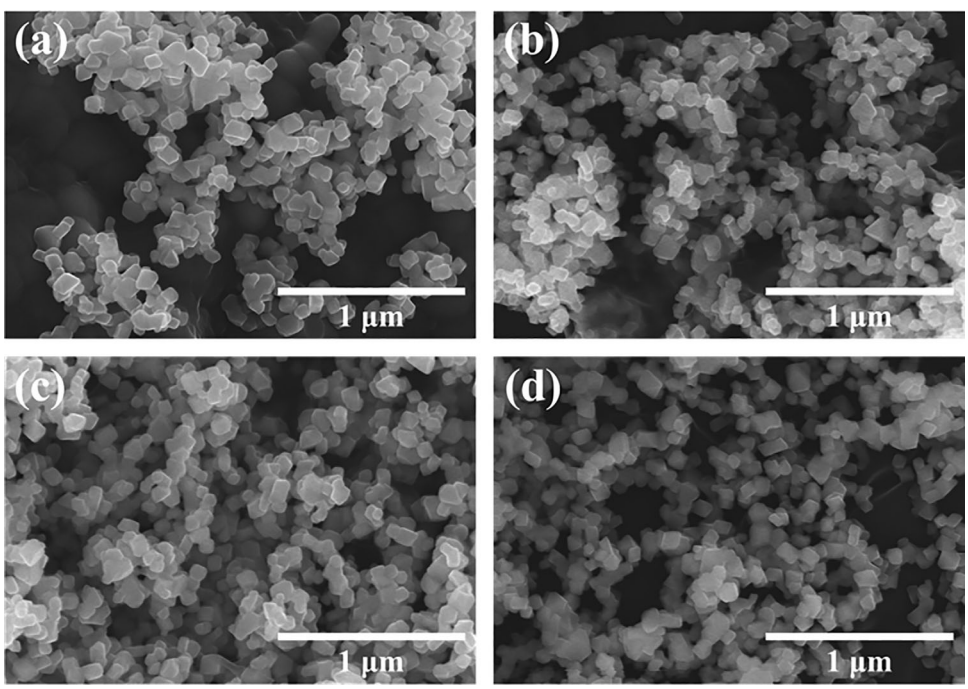

FIGURE 2 | FE-SEM images of the as-calcined powder for various La^{3+} concentrations: (a) $x = 0$, (b) $x = 0.05$, (c) $x = 0.1$, and (d) $x = 0.2$.

3 | Results and Discussion

Figure 2 shows FE-SEM micrographs of calcined powders with different La^{3+} doping concentrations. All the samples exhibited a loosely aggregated morphology composed of submicron-sized particles. The particles displayed irregular polyhedral shapes, typical of nanoscale powders produced via wet chemical methods. There was no evident change in morphology or powder dispersion with respect to La^{3+} concentration; all the powders remained uniformly dispersed with particle diameters of approximately 80 nm.

Figures 3 and 4 show the x-ray diffraction (XRD) patterns of the calcined powders and the sintered ceramics after SPS, respectively. All the diffraction peaks of both the powders and ceramics matched well with the Y_2O_3 phase (No. 86–1326) [39], indicating that the powders and ceramics have a cubic structure without any secondary phases. The XRD peak positions shifted slightly with increasing La^{3+} content owing to changes in the lattice constant. Additionally, the full width at half maximum (FWHM) of the characteristic peak of the powder with 20 at.% La^{3+} showed significant broadening, as Figure 3b shows, reflecting

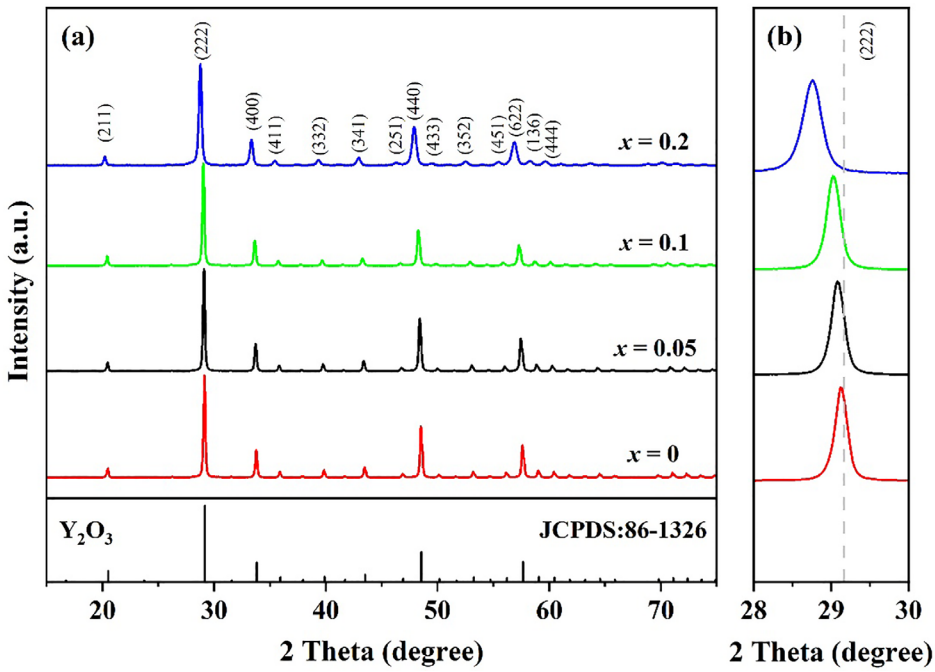

FIGURE 3 | (a) X-ray diffraction patterns of the calcined $(Er_{0.05}Y_{0.95-x}La_x)_2O_3$ powder for various La^{3+} concentrations; (b) magnified image of (222) peak.

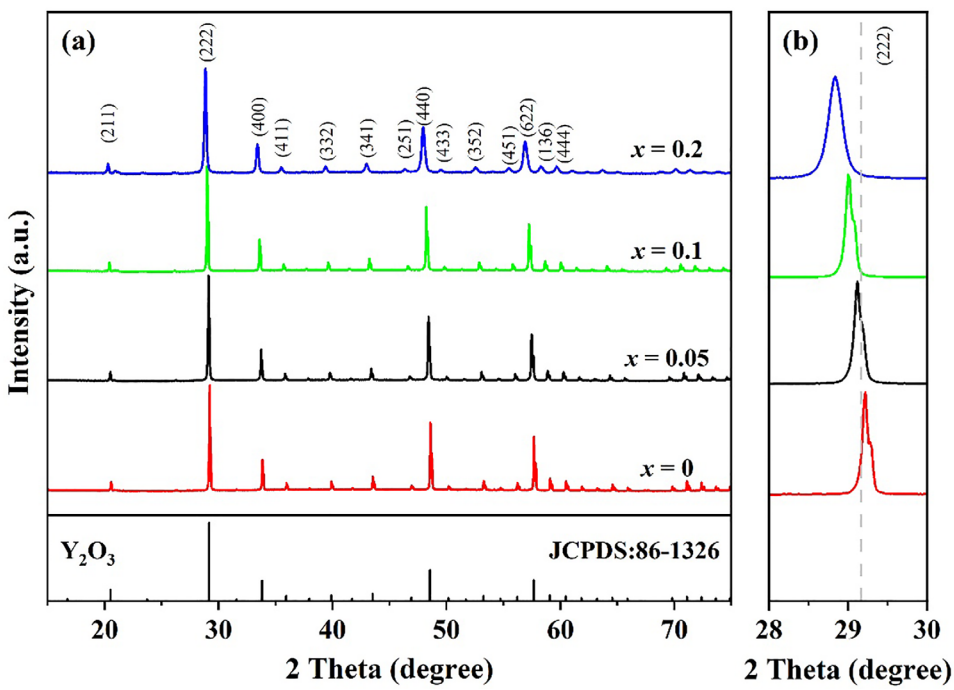

FIGURE 4 | (a) X-ray diffraction patterns of the as-sintered $(Er_{0.05}Y_{0.95-x}La_x)_2O_3$ ceramics for various La^{3+} concentrations; (b) magnified image of (222) peak.

internal lattice disorder that may contribute to increased emission bandwidth [39].

Using the Miller index (hkl) model and Bragg's law, the lattice parameter (a) of the cubic crystal can be calculated as follows:

$$d_{hkl} = \frac{a}{\sqrt{h^2 + k^2 + l^2}} \tag{1}$$

$$2\, d_{hkl}\, \sin\theta = \lambda \tag{2}$$

where d_{hkl} is the interplanar spacing, θ is the diffraction angle, λ is the X-ray wavelength, and (hkl) are the Miller indices of the diffraction plane. The lattice parameters of powders and ceramics are plotted as a function of La^{3+} content in Figure 5, revealing a linear increase with La^{3+} concentration, signifying successful

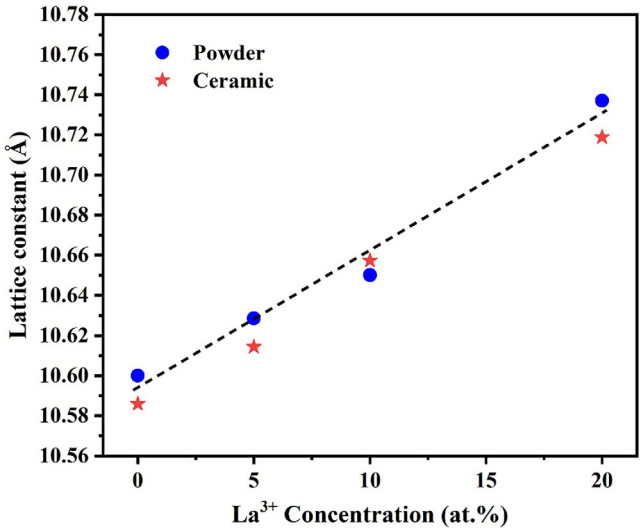

FIGURE 5 | Lattice constants as a function of the La^{3+} concentration for $(Er_{0.05}Y_{0.95-x}La_x)_2O_3$.

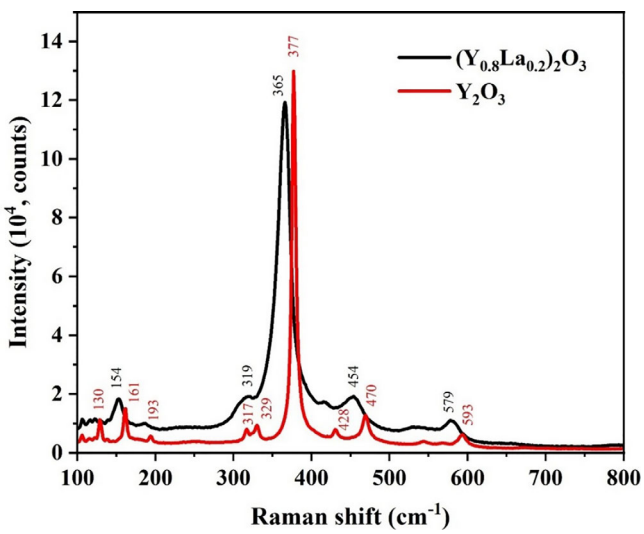

FIGURE 6 | Raman spectra of the undoped Y_2O_3 and $(Y_{0.8}La_{0.2})_2O_3$ powders.

incorporation of La^{3+} ions into the Y_2O_3 lattice and the formation of a single-phase solid solution.

Raman spectra of the calcined Y_2O_3 and $(Y_{0.8}La_{0.2})_2O_3$ powders are shown in Figure 6. The spectra of both samples matched well with the typical nature of cubic sesquioxides, but the spectrum of $(Y_{0.8}La_{0.2})_2O_3$ broadened and was slightly red shifted. The maximum phonon energies of the Y_2O_3 and $(Y_{0.8}La_{0.2})_2O_3$ powders were 593 and 579 cm^{-1}, indicating that incorporation of La^{3+} ions likely reduces non-radiative relaxation in the ceramic materials.

Figure 7a,b shows the sample images and in-line transmittance spectra of the $(Er_{0.05}Y_{0.95-x}La_x)_2O_3$ ceramics after SPS with a thickness of 1.2 mm. The in-line transmittance (T) can be expressed as a function of sample thickness and internal scattering and absorption losses, namely, $T = T_0 \exp[-(\alpha + \sigma)d]$, where α denotes the absorption coefficient, σ denotes the scattering coefficient, and d denotes the sample thickness. The theoretical transmittance (T_0) can be obtained from the Fresnel reflectance (R) as follows:

$$T_0 = (1 - R)^2 \tag{3}$$

$$R = \frac{(1 - n)^2}{(1 + n)^2} \tag{4}$$

where n denotes the refractive index dispersion of the undoped Y_2O_3 material [22, 40].

The in-line transmittance of the Er:Y_2O_3 ($x = 0$) ceramic was 82.1% at 2720 nm, which is comparable to the theoretical value of 82.6%. This corresponds to a loss coefficient of 0.05 cm^{-1}, which is closer to the laser quality requirements. The transmittance of the other three ceramics showed a decreasing trend with increasing La^{3+} content, and the ceramic with $x = 0.2$ exhibited a minimum transmittance of 80.8% with a corresponding loss coefficient of 0.18 cm^{-1}. Moreover, the transmittance of the ceramics decreased more significantly with La^{3+} content in the wavelength range below 1500 nm, notably at the excitation wavelength of 976 nm, mainly owing to residual pores within the ceramics.

The microstructural images of the polished ceramic surfaces are shown in Figure 8. No secondary phases were observed for any La^{3+} content, which corresponded to the XRD results shown in Figure 4. In Figure 8a, the sintered ceramic with 0 at.% La^{3+} concentration consists of extremely fine crystal grains. However, as shown in Figure 8b–d, the number of residual pores increased with increasing La^{3+} concentration. The average grain size of the ceramics decreased from 298 nm for Er:Y_2O_3 ceramic to 247, 187, and 131 nm for those containing 5, 10, and 20 at.% La^{3+} concentrations, respectively. This indicates that the decrease in average grain size may be attributed to La^{3+} ion acting as a sintering inhibitor [25, 41], leading to suppressed grain growth and an increased number of residual pores. One approach to further improve optical transmittance is to optimize the SPS sintering conditions, such as sintering temperature or applied pressure.

The SPSed samples were subjected to subsequent HIP processing at different temperatures to improve optical quality by removing residual pores. Figure 9 presents in-line transmittance spectra and corresponding photographs of the $(Er_{0.05}Y_{0.95-x}La_x)_2O_3$ ceramics after different HIP treatments. Compared with SPSed ceramics, post-HIP ceramics exhibited improved optical transparency. In the visible to near-infrared range, the in-line transmittance generally increased with increasing HIP temperature for $x = 0$, 0.05, and 0.1, attributed to the effective removal of residual pores. By contrast, the optical transmittance of the sample with $x = 0.2$ improved after HIP processing at 1200°C, while further increases in HIP temperature led to reduced optical transmittance. Notably, the transmittance of the sample treated by HIP at 1400°C decreased dramatically and became almost opaque.

Figure 10 illustrates the phase composition of $x = 0.2$ samples after varying HIP treatments. In Figure 10a, the SPSed sample treated at 1200°C remained a single cubic phase. However, increasing the HIP temperature introduced several new diffraction peaks

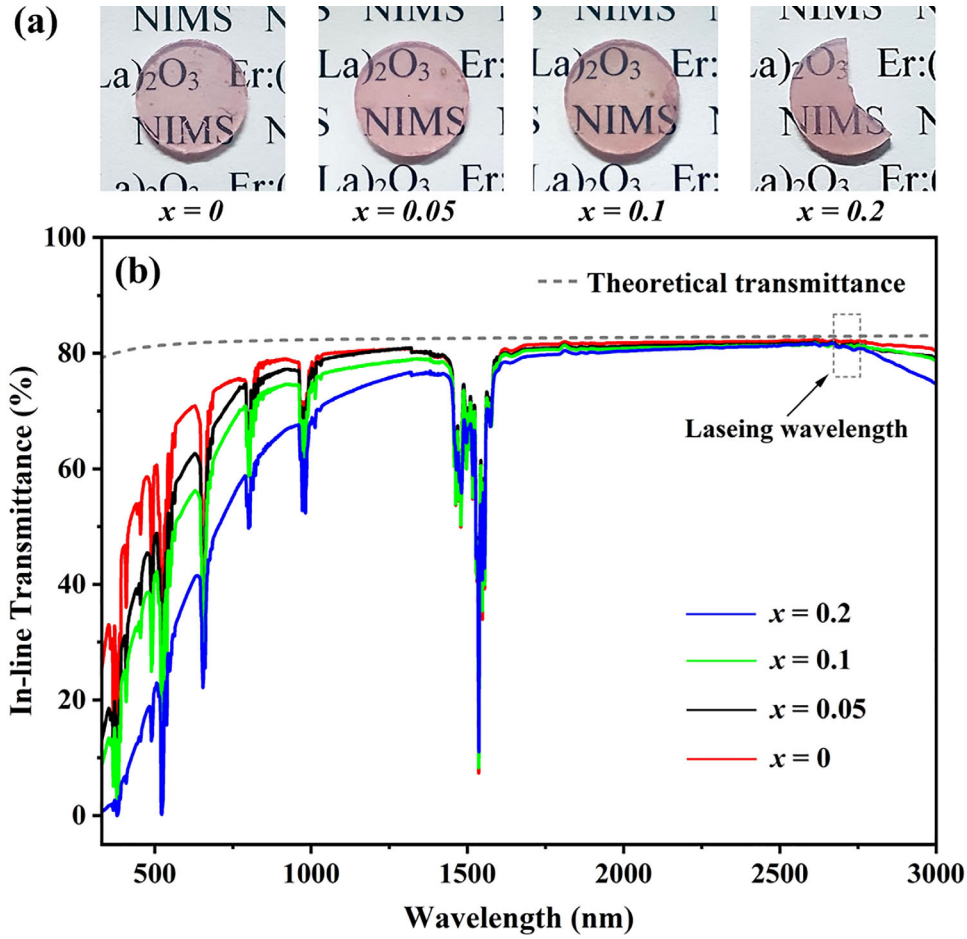

FIGURE 7 | (a) Sample images and (b) in-line transmittance spectra of the $(Er_{0.05}Y_{0.95-x}La_x)_2O_3$ ceramics for various La^{3+} concentrations after SPS.

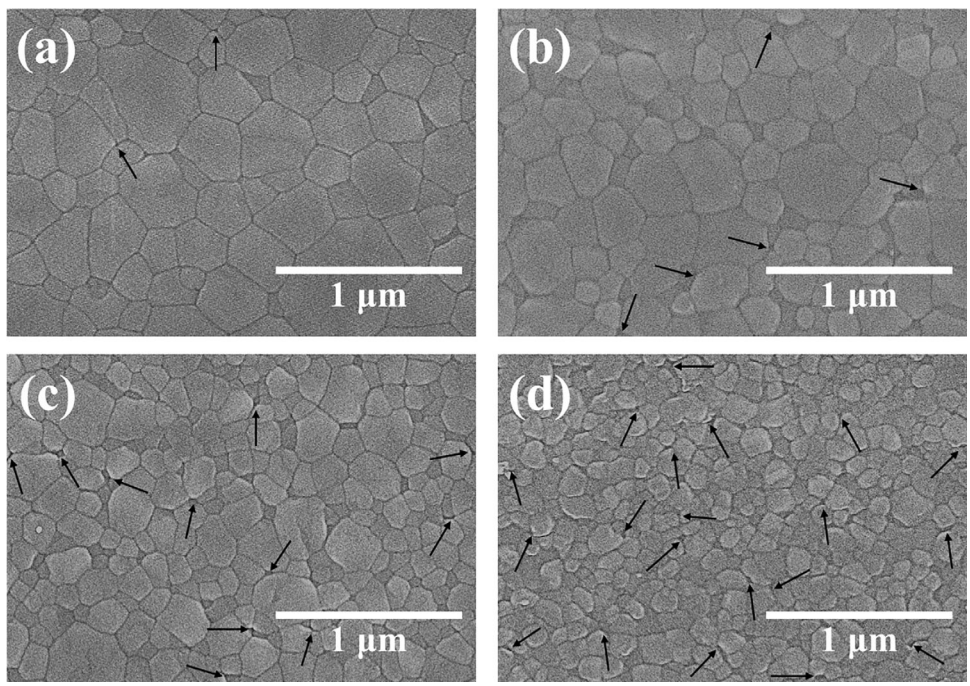

FIGURE 8 | FE-SEM images of the polished $(Er_{0.05}Y_{0.95-x}La_x)_2O_3$ ceramic surfaces for various La^{3+} concentrations: (a) $x = 0$, (b) $x = 0.05$, (c) $x = 0.1$, and (d) $x = 0.2$.

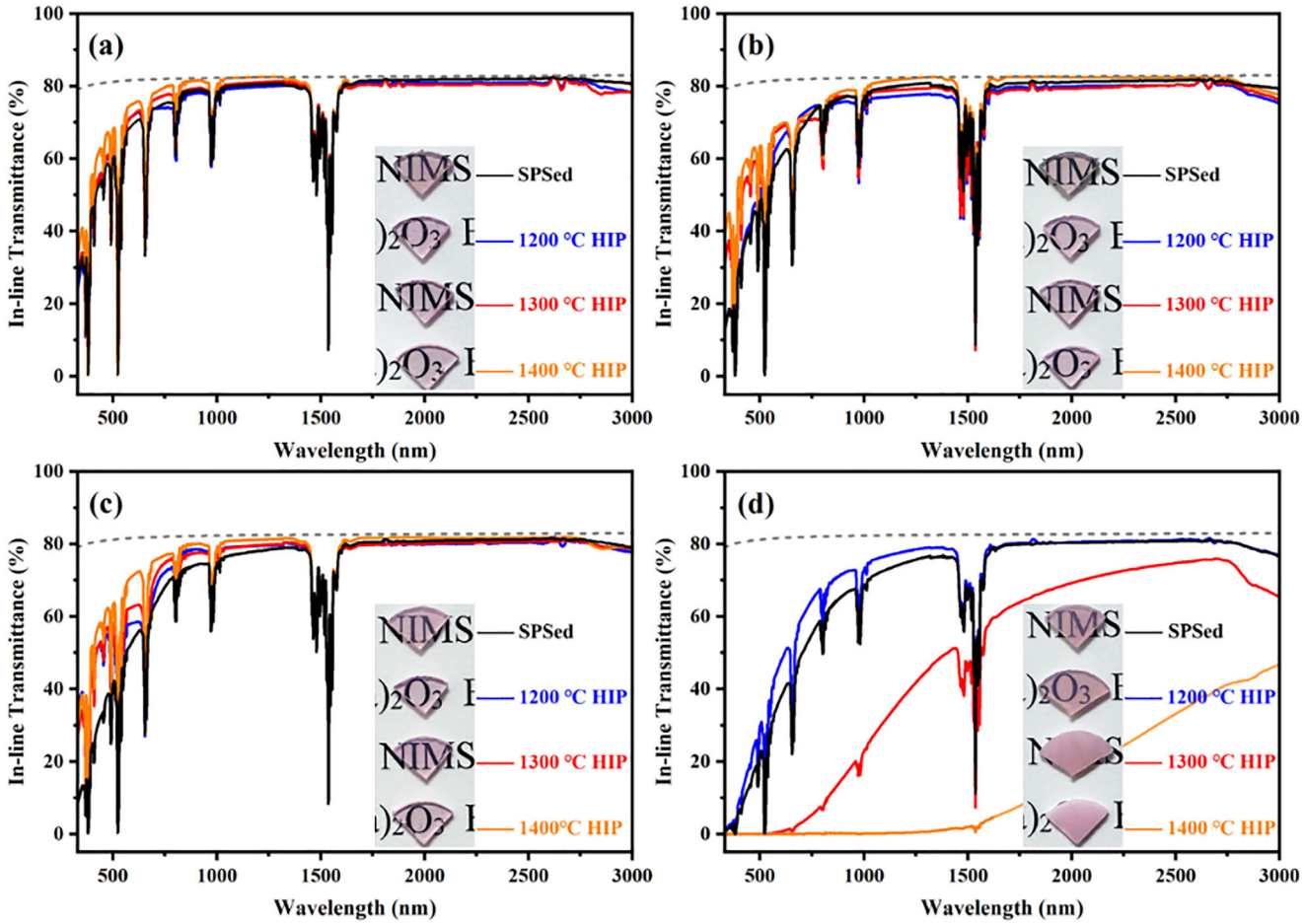

FIGURE 9 | In-line transmittance spectra of the $(Er_{0.05}Y_{0.95-x}La_x)_2O_3$ ceramics with corresponding photographs after different HIP treatments for various La^{3+} concentrations: (a) $x = 0$, (b) $x = 0.05$, (c) $x = 0.1$, and (d) $x = 0.2$.

in the XRD patterns. As shown in Figure 10b, these diffraction peaks were located at intermediate position between those of monoclinic Y_2O_3 phase (No. 90–4438) and La_2O_3 phase (No. 76–7413), suggesting the possible formation of a monoclinic $(Y,La)_2O_3$ phase during high-temperature HIP treatment. This secondary phase acts as a scattering center, leading to reduced optical transmittance. These results suggest that low-temperature sintering is essential for fabricating transparent ceramics with high La^{3+} concentrations.

The measured luminescence spectra in the mid-infrared range for the SPSed $(Er_{0.05}Y_{0.95-x}La_x)_2O_3$ ceramics before HIP treatment are shown in Figure 11a. The broad luminescence spectra span from 2580 to 3000 nm, corresponding to the $^4I_{11/2} \rightarrow {}^4I_{13/2}$ transition of Er^{3+} ions. With increasing La^{3+} content, the luminescence spectra became less structured and exhibited inhomogeneous broadening. Generally, two possible lasing modes were observed in the mid-infrared spectral region at 2710 nm and 2850 nm [22, 42]. For the most intense peak centered at around 2720 nm, the emission bandwidth (FWHM) of the sample with $x = 0.2$ reached approximately 17 nm compared with approximately 4 nm for the sample with $x = 0$. The incorporation of larger La^{3+} ions into the Y_2O_3 lattice induces local lattice distortion and modifies the crystal-field environment around the Er^{3+} ions. Consequently, the Stark splitting of the $^4I_{11/2}$ manifolds at 2720 nm may vary slightly among different Er^{3+} centers. The overlap of emissions resulting from these local crystal-field perturbations leads to enhanced inhomogeneous broadening of the mid-infrared luminescence band. For another intense peak band in the range of 2820–2880 nm shown in Figure 11b, the FWHM of the Er:$(Y_{0.8}La_{0.2})_2O_3$ ceramics broadened to approximately 18 nm. These results confirm that high La^{3+} incorporation effectively enhances spectral broadening of the mid-infrared emission, which is advantageous for developing ultrashort pulse lasers.

The luminescence decay curves from the $^4I_{11/2} \rightarrow {}^4I_{13/2}$ transition of Er^{3+} in the different samples are shown in Figure 12. These were fitted using the following function to evaluate the average lifetime:

$$I\ (t) = A_1 \exp\left(-\frac{t}{\tau_1}\right) + A_2 \exp\left(-\frac{t}{\tau_2}\right) \tag{5}$$

$$\tau_{ave} = \frac{A_1(\tau_1)^2 + A_2(\tau_2)^2}{A_1\tau_1 + A_2\tau_2} \tag{6}$$

where $A_1 + A_2 \approx 1$ and τ_{ave} denotes the average luminescence lifetime.

The average luminescence lifetimes were 3.3, 3.4, 3.6, and 3.8 ms for ceramics with $x = 0$, 0.05, 0.1, and 0.2, respectively. Interest-

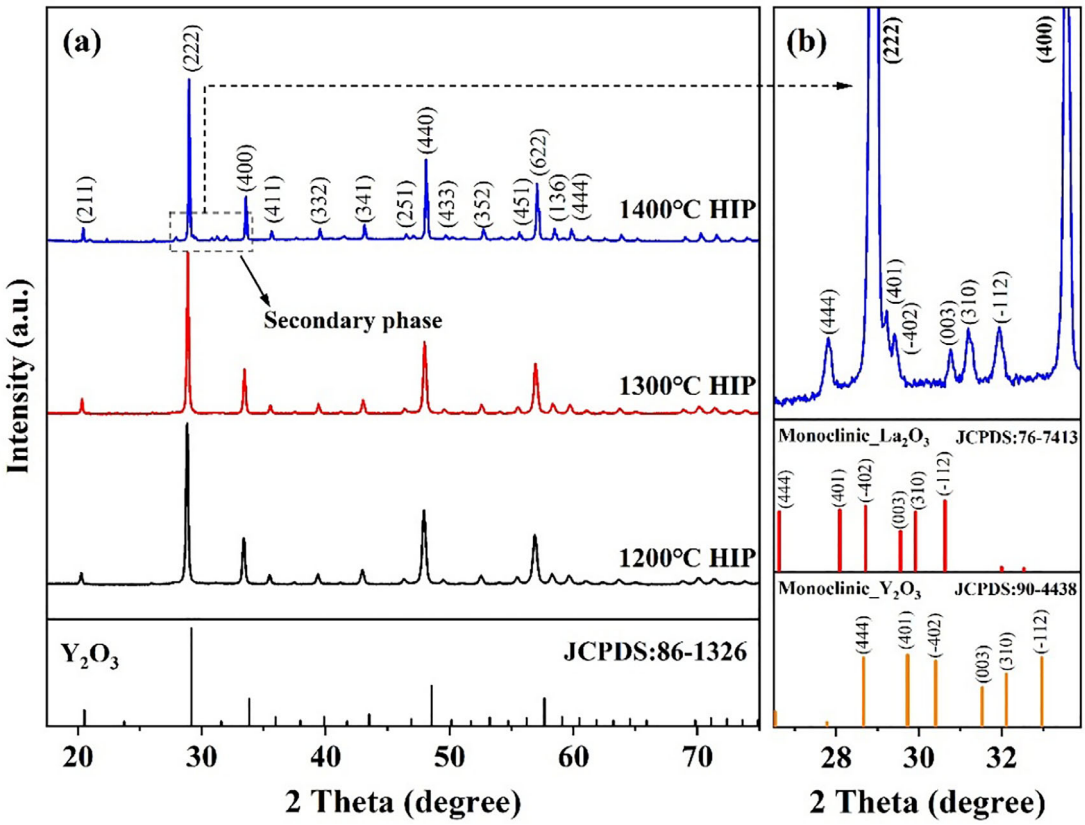

FIGURE 10 | (a) XRD patterns for the $(Er_{0.05}Y_{0.75}La_{0.2})_2O_3$ samples after HIP treatment at 1200°C, 1300°C, and 1400°C, respectively. (b) Magnified image of the XRD patterns for the sample treated at 1400°C.

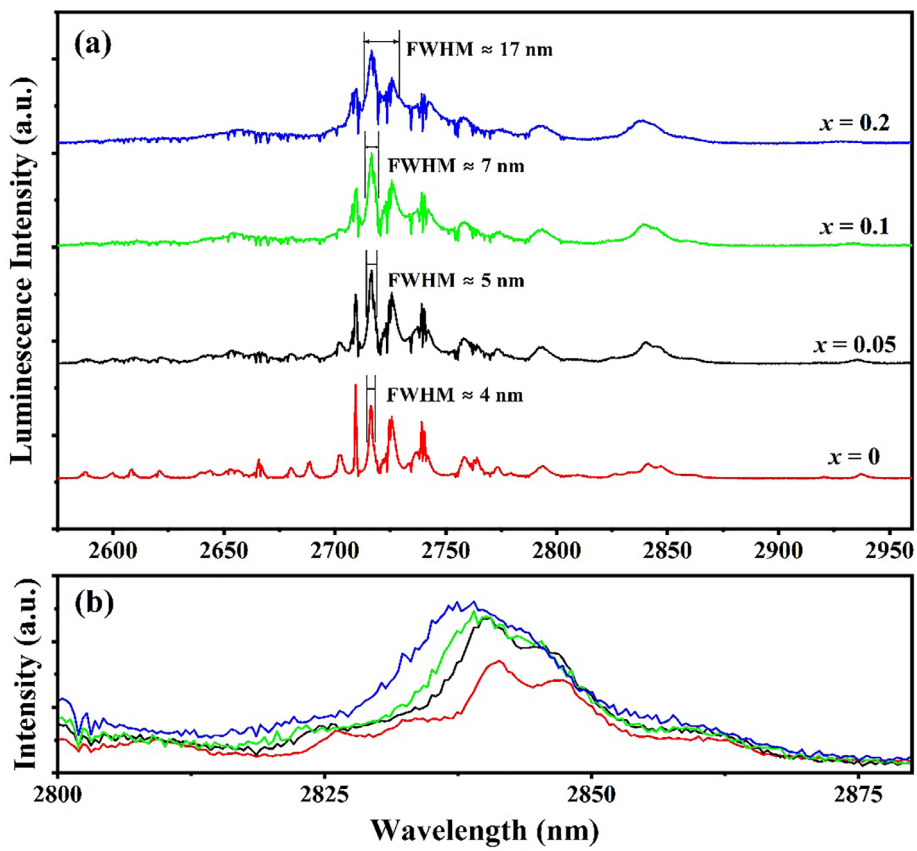

FIGURE 11 | Luminescence spectra of the $(Er_{0.05}Y_{0.95-x}La_x)_2O_3$ ceramics for various La^{3+} concentrations: (a) full spectra; (b) a close look at the 2800–2880 nm wavelength range.

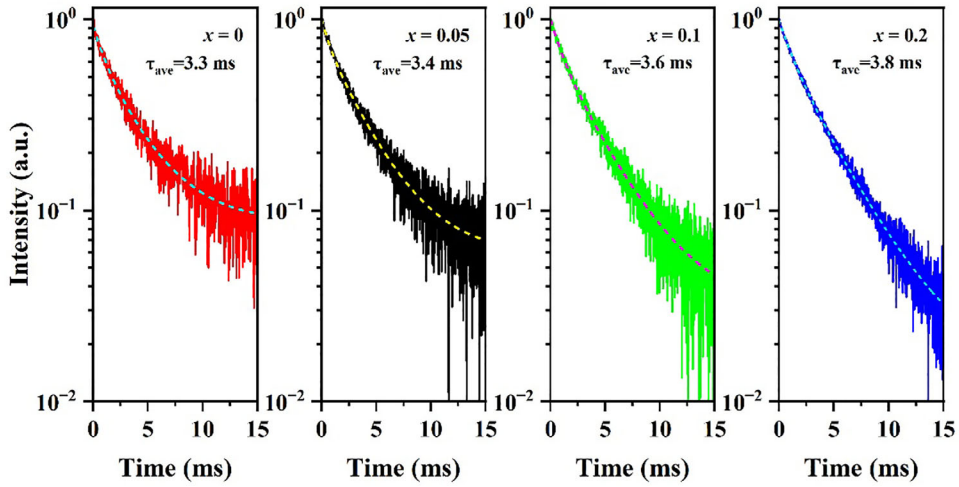

FIGURE 12 | Mid-infrared luminescence decay curves of the $(Er_{0.05}Y_{0.95-x}La_x)_2O_3$ ceramics for various La^{3+} concentrations.

ingly, the average lifetime increased with increasing La^{3+} content. We attribute this to the reduction in maximum phonon energy of ceramics, which suppresses multi-phonon relaxation and consequently enhances radiative efficiency at this wavelength. Notably, the $(Er_{0.05}Y_{0.75}La_{0.2})_2O_3$ ceramics exhibited a long luminescence lifetime of 3.8 ms and a broad emission bandwidth exceeding 17 nm, signifying higher luminescence emission capability than the other samples. These results suggest that increasing the La^{3+} concentration to 20 at.% can enhance the potential of these ceramics for ultrashort pulse mid-infrared laser applications. However, achieving the suppression of secondary phases at higher La^{3+} concentrations requires careful optimization of the fabrication process, including suitable powder synthesis, low-temperature SPS processing, and subsequent HIP treatment. We believe that further improvements in transmittance can be realized by optimizing these conditions, ultimately facilitating efficient laser operation.

4 | Conclusions

The combination of the co-precipitation method and SPS is an effective strategy for fabricating highly transparent $(Er_{0.05}Y_{0.95-x}La_x)_2O_3$ ceramics with x values of 0, 0.05, 0.1, and 0.2. SPS is currently the only practical method available for producing transparent ceramics with high La^{3+} concentrations. La^{3+} ions were incorporated into the Y_2O_3 lattice during the co-precipitation process, resulting in intrinsic disorder of the crystal field and a decrease in maximum phonon energy, which contributed to broadening of the emission spectra and extension of the luminescence lifetime. For the sample with $x = 0.2$, the emission spectral width at 2720 nm broadened to around 17 nm, while the luminescence lifetime of the $^4I_{11/2} \rightarrow {}^4I_{13/2}$ transition increased to 3.8 ms. However, the in-line transmittance at 2720 nm for the $x = 0.2$ sample decreased to 80.8% owing to formation of residual pores. Ultimately, further improvement in optical transmittance at the pump source wavelength was achieved by appropriate HIP treatment, which is significant for exploring more efficient ultrashort lasers in the mid-infrared region.

Acknowledgments

This study was supported by the JST FOREST Program (JPMJFR203S).

Conflicts of Interest

The authors declare no conflicts of interest.

Data Availability Statement

The data that support the findings of this study are available from the corresponding author upon reasonable request.

References

1. J. S. Liu, J. J. Liu, and Y. Tang, "Performance of a Diode End-Pumped Cr, Er: YSGG Laser at 2.79 μm," *Laser Physics* 18, no. 10 (2008): 1124–1127, https://doi.org/10.1134/S1054660X08100022.

2. Z. D. Fleischman and T. Sanamyan, "Spectroscopic Analysis of Er^{3+}:Y_2O_3 Relevant to 2.7 μm Mid-IR Laser," *Optical Materials Express* 6, no. 10 (2016): 3109–3118, https://doi.org/10.1364/ome.6.003109.

3. C. Kränkel, A. Uvarova, C. Guguschev, et al., "Rare-Earth Doped Mixed Sesquioxides for Ultrafast Lasers [Invited]," *Optical Materials Express* 12, no. 3 (2022): 1074–1091, https://doi.org/10.1364/ome.450203.

4. D. Yin, J. Wang, Y. Wang, et al., "Fabrication of Er:Y_2O_3 Transparent Ceramics for 2.7 μm Mid-Infrared Solid-state Lasers," *Journal of the European Ceramic Society* 40, no. 2 (2020): 444–448, https://doi.org/10.1016/j.jeurceramsoc.2019.09.051.

5. Z. Liu, A. Ikesue, and J. Li, "Research Progress and Prospects of Rare-Earth Doped Sesquioxide Laser Ceramics," *Journal of the European Ceramic Society* 41, no. 7 (2021): 3895–3910, https://doi.org/10.1016/j.jeurceramsoc.2021.02.026.

6. T. Südmeyer, C. Kränkel, C. R. E. Baer, et al., "High-Power Ultrafast Thin Disk Laser Oscillators and Their Potential for Sub-100-Femtosecond Pulse Generation," *Applied Physics B* 97, no. 2 (2009): 281–295, https://doi.org/10.1007/s00340-009-3700-z.

7. L. Basyrova, P. Loiko, W. Jing, et al., "Spectroscopy and Efficient Laser Operation Around 2.8 μm of Er:$(Lu,Sc)_2O_3$ Sesquioxide Ceramics," *Journal of Luminescence* 240 (2021): 118373, https://doi.org/10.1016/j.jlumin.2021.118373.

8. C. Kränkel, A. Uvarova, É. Haurat, et al., "Czochralski Growth of Mixed Cubic Sesquioxide Crystals in the Ternary System Lu_2O_3-

Sc_2O_3-Y_2O_3," *Acta Crystallographica Section B: Structural Science, Crystal Engineering and Materials* 77, no. 4 (2021): 550–558, https://doi.org/10.1107/S2052520621005321.

9. H. Wu, G. H. Pan, Z. Hao, et al., "Laser-Quality Tm:$(Lu_{0.8}Sc_{0.2})_2O_3$ Mixed Sesquioxide Ceramics Shaped by Gelcasting of Well-Dispersed Nanopowders," *Journal of the American Ceramic Society* 102, no. 8 (2019): 4919–4928, https://doi.org/10.1111/jace.16325.

10. W. Liu, D. Lu, R. Guo, et al., "Broadening of the Fluorescence Spectra of Sesquioxide Crystals for Ultrafast Lasers," *Crystal Growth & Design* 20, no. 7 (2020): 4678–4685, https://doi.org/10.1021/acs.cgd.0c00473.

11. S. Normani, P. Loiko, R. Maksimov, et al., "Solid-Solution Er:$(Sc,Y)_2O_3$ Transparent Ceramics: Optical Spectroscopy, Inhomogeneous Line Broadening, C_{3i} Sites and Mid-Infrared Laser Operation," *Optical Materials* 157 (2024): 116288, https://doi.org/10.1016/j.optmat.2024.116288.

12. S. Kalusniak, A. Uvarova, I. Arlt, et al., "Growth, Characterization, and Efficient Laser Operation of Czochralski- and Micro-Pulling-Down-Grown Yb^{3+} :$YScO_3$ Mixed Sesquioxides," *Optical Materials Express* 14, no. 2 (2024): 304–318, https://doi.org/10.1364/ome.513925.

13. R. D. Shannon, "Revised Effective Ionic Radii and Systematic Studies of Interatomie Distances in Halides and Chaleogenides," *Acta Crystallographica Section A, Crystal Physics, Diffraction, Theoretical and General Crystallography* 32, no. 5 (1976): 751–767, https://doi.org/10.1107/S0567739476001551.

14. Y. Q. Jia, "Crystal Radii and Effective Ionic Radii of the Rare Earth Ions," *Journal of Solid State Chemistry* 187, no. 1 (1991): 184–187, https://doi.org/10.1016/0022-4596(91)90388-X.

15. Z. Sun, G. Liu, Z. Fu, T. Sheng, Y. Wei, and Z. Wu, "Nanostructured La_2O_3: Yb^{3+}/Er^{3+}: Temperature Sensing, Optical Heating and Bio-Imaging Application," *Materials Research Bulletin* 92 (2017): 39–45, https://doi.org/10.1016/j.materresbull.2017.04.005.

16. K. A. Irshad, P. Anees, R. Rajitha, et al., "Anomalous Lattice Compression in the Hexagonal La_2O_3—A High Pressure X-ray Diffraction, Raman Spectroscopy and First Principle Study," *Journal of Alloys and Compounds* 822 (2020): 153657, https://doi.org/10.1016/j.jallcom.2020.153657.

17. Q. Yi, S. Zhou, H. Teng, H. Lin, X. Hou, and T. Jia, "Structural and Optical Properties of Tm:Y_2O_3 Transparent Ceramic With La_2O_3, ZrO_2 as Composite Sintering Aid," *Journal of the European Ceramic Society* 32, no. 2 (2012): 381–388, https://doi.org/10.1016/j.jeurceramsoc.2011.09.015.

18. Q. H. Yang, J. Ding, H. W. Zhang, and J. Xu, "Investigation of the Spectroscopic Properties of Yb^{3+}-Doped Yttrium Lanthanum Oxide Transparent Ceramic," *Optics Communication* 273, no. 1 (2007): 238–241, https://doi.org/10.1016/j.optcom.2006.12.035.

19. S. Li, X. Zhu, J. Li, et al., "Fabrication of 5 at.% Yb:$(La_{0.1}Y_{0.9})_2O_3$ Transparent Ceramics by Chemical Precipitation and Vacuum Sintering," *Optical Materials* 71 (2017): 56–61, https://doi.org/10.1016/j.optmat.2016.06.017.

20. Y. Liu, C. Liu, X. Qin, et al., "Fabrication and Luminescent Properties of Highly Transparent Er:Y_2O_3 Ceramics by Hot Pressing Sintering," *Materials* 16, no. 13 (2023): 4504, https://doi.org/10.3390/ma16134504.

21. Y. Sun, Q. Yang, H. Wang, Q. Zhang, and Y. Shao, "Preparation and Mid-Infrared 2.7 μm Luminescence Property of High Content Er^{3+}-Doped $(Y_{0.9}La_{0.1})_2O_3$ Transparent Ceramics Pumped at 980 Nm," *Ceramics International* 44, no. 2 (2018): 1812–1816, https://doi.org/10.1016/j.ceramint.2017.10.115.

22. S. Balabanov, P. Loiko, L. Basyrova, et al., "Mid-Infrared Laser Operation of $(Er_{0.07}La_{0.10}Y_{0.83})_2O_3$ Sesquioxide Ceramic," *Laser Physics Letters* 20, no. 4 (2023): 045801, https://doi.org/10.1088/1612-202X/acbce4.

23. J. Coutures and M. Foex, "Etude à Haute Température Du Diagramme D'equilibre Du Système Formé par Le Sesquioxyde De lanthane avec Le Sesquioxyde D'yttrium," *Journal of Solid State Chemistry* 11, no. 4 (1974): 294–300, https://doi.org/10.1016/S0022-4596(74)80034-4.

24. W. H. Rhodes, "Controlled Transient Solid Second-Phase Sintering of Yttria," *Journal of the American Ceramic Society* 64, no. 1 (1981): 13–19, https://doi.org/10.1111/j.1151-2916.1981.tb09551.x.

25. S. S. Balabanov, Y. V. Bykov, S. V. Egorov, et al., "Yb:$(Y,La)_2O_3$ Laser Ceramics Produced by Microwave Sintering," *Quantum Electronics* 43, no. 4 (2013): 396–400, https://doi.org/10.1070/qe2013v043n04abeh015137.

26. L. Zhang, J. Yang, H. Yu, and W. Pan, "High Performance of La-Doped Y_2O_3 Transparent Ceramics," *Journal of Advanced Ceramics* 9, no. 4 (2020): 493–502, https://doi.org/10.1007/s40145-020-0392-7.

27. O. V. Chudinovych, O. R. Andrievskaya, J. D. Bogatyryova, V. V. Kovylyaev, and O. I. Bykov, "Phase Equilibria in the La_2O_3-Y_2O_3-Nd_2O_3 System at 1500°C," *Journal of the European Ceramic Society* 41, no. 13 (2021): 6606–6616, https://doi.org/10.1016/j.jeurceramsoc.2021.06.017.

28. Y. Wu, "Nanostructured Transparent Ceramics With an Anisotropic Crystalline Structure," *Optical Materials Express* 4, no. 10 (2014): 2026–2031, https://doi.org/10.1364/OME.4.002026.

29. A. Wagner, B. Ratzker, S. Kalabukhov, M. Sokol, and N. Frage, "Residual Porosity and Optical Properties of Spark Plasma Sintered Transparent Polycrystalline Cerium-Doped YAG," *Journal of the European Ceramic Society* 39, no. 4 (2019): 1436–1442, https://doi.org/10.1016/j.jeurceramsoc.2018.11.006.

30. H. Furuse, N. Horiuchi, and B. N. Kim, "Transparent Non-Cubic Laser Ceramics With Fine Microstructure," *Scientific Reports* 9, no. 1 (2019): 10300, https://doi.org/10.1038/s41598-019-46616-8.

31. H. Furuse, Y. Mochizuki, D. Kato, K. Morita, B. N. Kim, and T. S. Suzuki, "Strontium Fluorapatite (S-FAP) Nano-Grained Laser Ceramics," *Scripta Materialia* 241 (2024): 115881, https://doi.org/10.1016/j.scriptamat.2023.115881.

32. H. Furuse, K. Takimoto, S. Koizumi, and H. Sone, "Fluorescence and Laser Properties of Nd-doped $(Ca_{0.5}Sr_{0.5})_{10}(PO_4)_6F_2$ Ceramics," *Optical Materials Express* 16, no. 4 (2026): 992–1000, https://doi.org/10.1364/OME.591337.

33. H. Furuse, S. Nakasawa, H. Yoshida, et al., "Transparent Ultrafine Yb^{3+}:Y_2O_3 Laser Ceramics Fabricated by Spark Plasma Sintering," *Journal of the American Ceramic Society* 101, no. 2 (2018): 694–702, https://doi.org/10.1111/jace.15232.

34. R. Yasuhara, H. Uehara, W. Yao, H. Chen, S. Tokita, and H. Furuse, "Dy-doped Y_2O_3 Transparent Ceramics as a Mid-Infrared Laser Medium and Saturable Absorber," *Optical Materials Express* 10, no. 11 (2020): 2998–3006, https://doi.org/10.1364/OME.409848.

35. L. Liu, K. Morita, T. S. Suzuki, and B.-N. Kim, "Effect of the Heating Rate on the Spark-Plasma-Sintering (SPS) of Transparent Y_2O_3 Ceramics: Microstructural Evolution, Mechanical and Optical Properties," *Ceramics* 4, no. 1 (2021): 56–69, https://doi.org/10.3390/ceramics4010006.

36. H. Furuse, D. Ueno, K. Omata, M. Imai, and S. Tokita, "Mid-Infrared Fine-Grained Er:Y_2O_3 Laser Ceramics Fabricated by Spark Plasma Sintering," *Ceramics International* 50, no. 22 (2024): 46925–46931, https://doi.org/10.1016/j.ceramint.2024.09.044.

37. T. Entradas, J. F. Cabrita, S. Dalui, M. R. Nunes, O. C. Monteiro, and A. J. Silvestre, "Synthesis of Sub-5 Nm Co-doped SnO_2 Nanoparticles and Their Structural, Microstructural, Optical and Photocatalytic Properties," *Materials Chemistry and Physics* 147, no. 3 (2014): 563–571, https://doi.org/10.1016/j.matchemphys.2014.05.032.

38. M. Musharaf, S. Karamat, M. U. Hassan, et al., "Solubility Enhancement of Fe in ZnO Nanoparticles Prepared by Co-Precipitation Method," *Journal of Superconductivity and Novel Magnetism* 34, no. 10 (2021): 2633–2642, https://doi.org/10.1007/s10948-021-05904-z.

39. C. Kränkel, "Rare-Earth-Doped Sesquioxides for Diode-pumped High-Power Lasers in the 1-, 2-, and 3-μm Spectral Range," *IEEE Journal of*

Selected Topics in Quantum Electronics 21, no. 1 (2015): 250–262, https://doi.org/10.1109/JSTQE.2014.2346618.

40. Y. Nigara, "Measurement of the Optical Constants of Yttrium Oxide," *Japanese Journal of Applied Physics* 7, no. 4 (1968): 404–408, https://doi.org/10.1143/JJAP.7.404.

41. J. Wang, F. Zhang, F. Chen, et al., "Effect of Y_2O_3 and La_2O_3 on the Sinterability of γ-AlON Transparent Ceramics," *Journal of the European Ceramic Society* 35, no. 1 (2015): 23–28, https://doi.org/10.1016/j.jeurceramsoc.2014.07.016.

42. R. Maksimov, V. Shitov, V. Osipov, et al., "Fabrication, Microstructure and Mid-Infrared Luminescence of Er:$(Sc_xY_{1-x})_2O_3$ Transparent Ceramics," *Optical Materials* 137 (2023): 113542, https://doi.org/10.1016/j.optmat.2023.113542.